

A single serine in the CC3 region of STIM1 is critical for STIM1-Orai1 binding and CRAC channel activation

Tao Yu¹, Xi Li¹, Huajing Liu¹, Jing Jin¹, Qianqian Luo¹, Shengjie Li¹, and Jun He¹

¹Tongji Medical College of Huazhong University of Science and Technology

July 8, 2022

Abstract

Background and purpose: Store-operated Ca²⁺ entry (SOCE) is important for the function of many cell types. It is controlled by the interaction between ER Ca²⁺ sensor STIM1 and the plasma membrane Ca²⁺ channel Orai1. CAD of STIM1 is required for SOCE. It contains two putative coiled-coil regions (CC2 and CC3). The role of CC3 remains to be elucidated. **Experimental approach:** various plasmids carrying different fluorescent protein genes were constructed for better understanding the influence of S417G mutation in CC3 on SOCE activation; Confocal imaging system, calcium imaging technique and FRET technique were employed to examine the actions of 2-APB on the interaction between STIM1 C terminus and Orai1. **Key results:** Single-point mutation of the residue (S417G) abolishes STIM1 C-terminus interactions with Orai1. Mutation of S417 also abolished CAD-Orai1 binding and Orai1 channel activation, eliminated STIM1 puncta formation and co-localization with Orai1 and SOCE. 2-APB were found to restore the binding of STIM1 C-terminus mutant(S417G) to Orai1 and dose-dependently activated Orai1 channel. Both CBD and NBD of Orai1 is required for 2-APB-induced coupling between Orai1 and STIM1 C terminus mutant(S417G) and CRAC channel activation. We also demonstrated 2-APB lead to delayed activation of Orai1-K85E channel, although Orai1-K85E obviously impair 2-APB-induced STIM1 C-terminus mutant(S417G)-Orai1 coupling. **Conclusions and implications:** Our data suggest that S417 in the CC3 domain of STIM1 is critical for STIM1-Orai1 binding and CRAC channel activation. We also proposed experimental models of combined STM1 or Orai1 mutants with 2-APB to better understand the activation mechanism of CRAC.

A single serine in the CC3 region of STIM1 is critical for STIM1-Orai1 binding and CRAC channel activation

Tao Yu², Xi Li¹, Huajing Liu¹, Jing Jin¹, Qianqian Luo¹, Shengjie Li¹, Jun He^{1*}

1. Division of Histology and Embryology, School of Basic Medical Sciences, Tongji Medical College, Huazhong University of Science and Technology, Wuhan, China
2. Department of Clinical Laboratory, Wuhan Children's Hospital(Wuhan Maternal and Child Healthcare Hospital), Tongji Medical College, Huazhong University of Science and Technology, Wuhan, China

Address correspondence to: Jun He, Division of Histology and Embryology, School of Basic Medicine, Tongji Medical College, Huazhong University of Science and Technology, Wuhan 430030, China, Tel. 86-27-83692612; E-Mail: junhe@mails.tjmu.edu.cn

Running Title: S417 is required for STIM1-Orai1 binding and channel activation

Keywords: SOCE; SOCs; CRAC; 2-Aminoethyldiphenyl borate; STIM1; Orai1; Confocal imaging; FRET

Abbreviations: SOCE, store-operated Ca^{2+} entry; 2-APB, 2-aminobiphenylborate; $[\text{Ca}^{2+}]_i$, intracellular Ca^{2+} concentration; STIM1, stromal interaction molecule 1; SOCs, store-operated channels; CRAC, calcium release-activated channels; I_{CRAC} , Ca^{2+} release-activated Ca^{2+} current; IP3, inositol 1,4,5-triphosphate; FRET, fluorescence resonance energy transfer

Data Availability Statement: The data that support the findings of this study are openly available in [repository name] at [http://doi.org/\[doi\]](http://doi.org/[doi]), reference number [reference number].

Summary

Background and purpose: Store-operated Ca^{2+} entry (SOCE) is important for the function of many cell types. It is controlled by the interaction between ER Ca^{2+} sensor STIM1 and the plasma membrane Ca^{2+} channel Orai1. CAD of STIM1 is required for SOCE. It contains two putative coiled-coil regions (CC2 and CC3). The role of CC3 remains to be elucidated.

Experimental approach: various plasmids carrying different fluorescent protein genes were constructed for better understanding the influence of S417G mutation in CC3 on SOCE

activation; Confocal imaging system, calcium imaging technique and FRET technique were employed to examine the actions of 2-APB on the interaction between STIM1 C terminus and Orai1.

Key results: Single-point mutation of the residue (S417G) abolishes STIM1 C-terminus interactions with Orai1. Mutation of S417 also abolished CAD-Orai1 binding and Orai1 channel activation, eliminated STIM1 puncta formation and co-localization with Orai1 and SOCE. 2-APB were found to restore the binding of STIM1 C-terminus mutant(S417G) to Orai1 and dose-dependently activated Orai1 channel. Both CBD and NBD of Orai1 is required for 2-APB-induced coupling between Orai1 and STIM1 C terminus mutant(S417G) and CRAC channel activation. We also demonstrated 2-APB lead to delayed activation of Orai1-K85E channel, although Orai1-K85E obviously impair 2-APB-induced STIM1 C-terminus mutant(S417G)-Orai1 coupling.

Conclusions and implications: Our data suggest that S417 in the CC3 domain of STIM1 is critical for STIM1-Orai1 binding and CRAC channel activation. We also proposed experimental models of combined STM1 or Orai1 mutants with 2-APB to better understand the activation mechanism of CRAC.

Introduction

Store-operated Ca^{2+} entry (SOCE) are the major route of Ca^{2+} entry in both excitable and especially in non-excitabile cells, and play important roles in the control of gene expression, cell growth and differentiation, motility, secretion, tissue and organ development, and the immune response (Feske, 2010; Parekh & Putney, 2005; Prakriya & Lewis, 2015; Shim, Tirado-Lee & Prakriya, 2015). Abnormal SOCE has been associated with different human disorders. Loss-of-function mutations in Orai1 and STIM1 genes cause CRAC channelopathies, involving immunodeficiency and autoimmunity, muscular hypotonia, ectodermal dysplasia, and mydriasis(Feske et al., 2006; Lacruz & Feske, 2015; Picard, Mccarl, Papolos, Khalil & Feske, 2009). In contrast, STIM1 and Orai1 gain-of-function mutations were found in patients with tubular aggregate myopathy (TAM) and Stormorken syndrome (STRMK)(Böhm et al., 2013; Misceo et al., 2014; Morin et al., 2020; Morin et al., 2014; Nesin et al., 2014). In addition, SOCE play important roles in the pathophysiology of

cardiovascular diseases, thrombus formation, tumor cell metastasis, and the pathogenesis of acute pancreatitis (Braun et al., 2009; Lee & Papachristou, 2019; Lu, Zhang, Su, Zhou & Xu, 2022; Varga-Szabo et al., 2008; Yang, Zhang & Huang, 2009; Zhu, Yu, Liu, Jin & He, 2018), etc.

Regulation of SOCE is a highly choreographed process that involves a complex conformational rearrangement of STIM1 proteins (Hogan, Lewis & Rao, 2009; Prakriya & Lewis, 2015; Shaw, Qu, Hoth & Feske, 2013). In resting cells replete with Ca^{2+} , STIM1 is distributed diffusely throughout the ER in an inactive state (Baba et al., 2006; Wu, Covington & Lewis, 2014; Zhang et al., 2005a). After ER Ca^{2+} depletion, Ca^{2+} release from the luminal Ca^{2+} -binding EF hand, leading to the unfolding of the EF-sterile α motif (SAM) domain, and the conformational extension of the cytoplasmic STIM1 C terminus (STIM1-CT) (Korzeniowski, Manjarrés, Varnai & Balla, 2010; Muik et al., 2011; Yu, Sun, Hubrack, Selvaraj & Machaca, 2013; Zhou et al., 2013). STIM1-CT contains three coiled-coil domains: CC1 (residues 238–343), CC2 (residues 363–389), and CC3 (residues 399–423). CC2 and CC3 are located in a ~ 100 amino acids region in STIM1-CT variously termed CRAC activation domain (CAD; residues 342–448) or STIM1-Orai1 activating region (SOAR; residues 344–442), or coiled-coil domain b9 (CCb9, amino acids 339–446) (Kawasaki, Lange & Feske, 2009; Park et al., 2009; Soboloff, Rothberg, Madesh & Gill, 2012; Yuan, Zeng, Dorwart, Choi, Worley & Muallem, 2009). Conformational extension of STIM1-CT exposes its polybasic domain at the distal end (Korzeniowski, Manjarrés, Varnai & Balla, 2010; Muik et al., 2011; Yu, Sun, Hubrack, Selvaraj & Machaca, 2013; Zhou et al., 2013). This polybasic domain facilitates the recruitment of STIM1 oligomers to ER–PM junctions by interacting with acidic phospholipids in the PM, where Orai1 accumulates in the areas of plasma membrane apposed STIM1 puncta, and CAD or SOAR segment of STIM1 bind to C and N termini of Orai1 protein (Korzeniowski, Manjarrés, Varnai & Balla, 2010; Liou, Fivaz, Inoue & Meyer, 2007; Muik et al., 2011; Park et al., 2009; Yuan, Zeng, Dorwart, Choi, Worley & Muallem, 2009; Zhou et al., 2013), which is sufficient to activate CRAC channels and induce constitutive Ca^{2+} influx (Kawasaki, Lange & Feske, 2009; Park et al., 2009; Soboloff, Rothberg, Madesh & Gill, 2012; Yuan, Zeng, Dorwart, Choi, Worley & Muallem, 2009). The structurally best defined region in CAD is CC2 that establishes the binding interactions with

Orai1(Stathopoulos et al., 2013). Although recent studies have shown that a coiled-coil clamp involving the CC1 and CC3 domains is essential in controlling STIM1 activation, the role of CC3 remains to be elucidated(Fahrner et al., 2014; Maus et al., 2015; Muik et al., 2011; Rathner et al., 2021).

Here we show that a single serine residue in CC3 segment is absolutely required for STIM1-CT binding to Orai1. Mutation of S417 in CC3 hinders STIM1 puncta formation and impairs CAD-Orai1 binding, thereby abolishing CRAC channel activation. 2-Aminoethoxydiphenyl borate (2-APB), a popular pharmacological agent in the study of CRAC/store-operated channels can restore the binding of STIM1-CT mutant (S417G) to Orai1 and activate Orai1 channel in a dose-dependent manner. Our data indicated that S417 in CC3 domain of STIM1 might be a crucial element for STIM1 function and activation of CRAC and CC3 domain of STIM1 play an essential role for these processes. We also present a new finding about 2-APB's action on CRAC channel, which provides a solid base for better understanding of SOCE activation.

Materials and Methods

Cell culture and transfection. HeLa cells (American Type Culture Collection, Manassas, VA, USA) were cultured in Dulbecco's modified Eagle's medium (DMEM) containing 10% heat-inactivated fetal bovine serum, 50 U/ml penicillin, and 50 mg/ml streptomycin. Cells were maintained at 37 °C in a humidified incubator set at 5% CO₂ and were seeded on 30-mm round glass coverslips in a 6-well plate. On the following day, cells were transfected with plasmids using Lipofectamine 2000 (Invitrogen, Carlsbad, CA, USA) according to the manufacturer's instructions; 6 h later, the medium was replaced with complete DMEM and cells were cultured overnight. Cells were used for analyses 48 h later.

Plasmid construction. Human STIM1 (accession number NM_003156) tagged at the N terminus with pHluorin (pHluorin-STIM1) was a gift from Dr. P.Y. Xu (Institute of Biophysics, Chinese Academy of Sciences) and CMV-R-GECO1.2 was a gift from Robert Campbell (Addgene plasmid # 45494). The pHluorin was replaced with ECFP or EYFP to generate ECFP-STIM1 or EYFP-STIM1 plasmids. For double-labeled STIM1 constructs,

YFP was cloned into the XhoI and HindIII restriction sites of pECFP-N1 and STIM1 fragments were introduced into the EcoRI and BamHI sites [amino acid (a.a.) 233–685, 233–671, 233–474, and 342–448]. The fusion proteins Orai1-YFP and Orai1-mKate were generated by amplifying full-length Orai1 via PCR and cloning the fragments between the EcoRI and BamHI restriction sites of pEYFP-N1 and mKate-N1 vectors, respectively (Clontech, Mountain View, CA, USA). An N-terminal Orai1 deletion mutant (Orai1- Δ N-mKate, Δ a.a. 90–301) was cloned by PCR into the mKate-N1 internal EcoRI and BamHI restriction sites. A C-terminal Orai1 deletion mutant (Orai1- Δ C-mKate, Δ a.a. 1–272) was similarly constructed. A C-terminally tagged N-terminal binding domain (NBD) Orai1 deletion mutant (Orai1- Δ NBD, Δ a.a. 73–85) was cloned into the EcoRI and BamHI restriction sites of mKate-N1 and pEYFP-N1 expression vectors (Clontech). A CBD Orai1 deletion mutant (Orai1- Δ CBD, Δ a.a. 272–292) was prepared as described above. Orai1 and STIM1 point mutants were generated using the QuikChange XL site-directed mutagenesis kit (Stratagene, La Jolla, CA, USA). The integrity of all clones was confirmed by sequence analysis.

Solutions and chemicals. For confocal imaging experiments, we used standard extracellular Ringer's solution containing the following (in mM): 150 NaCl, 5 KCl, 1.8 CaCl₂, 1 MgCl₂, 8 glucose, and 10 HEPES (pH 7.4, adjusted with NaOH). CaCl₂ was replaced with 1 mM EGTA and 2 mM MgCl₂ in Ca²⁺-free Ringer's solution. Stock solutions of thapsigargin and 2-APB were prepared in Me₂SO at a concentration of 1 mM. Fura-2/AM was purchased from Invitrogen. Unless otherwise specified, all reagents and chemicals were from Sigma-Aldrich (St. Louis, MO, USA).

Confocal microscopy and FRET measurements. The Olympus FV1000 laser scanning confocal microscopy system (Olympus, Tokyo, Japan) was used for experiments. Coverslips seeded with HeLa cells transiently transfected with various vectors were placed in a perfusion chamber on the stage of an Olympus IX81 inverted microscope. Images were acquired at room temperature with a 40 \times or 60 \times oil objective (N.A. 1.4; Olympus), and images were analyzed with Fluoview software (Olympus). CFP, YFP, and mKate/R-GECO1.2 were excited

at 405, 514, and 559 nm, respectively.

For FRET experiments, CFP, YFP, and FRET fluorescence was collected with the following parameters: CFP: 405 nm excitation, 450–510 nm emission; YFP: 514 nm excitation, 540–625 nm emission; FRET: 405 nm excitation, 540–625 nm emission. Image acquisition was performed using FV10-ASW Ver.3.1 software. Image analysis was performed with Matlab7.0 software to calculate N-FRET (Normalized FRET) according to the equation: $NFRET = (I_{DA} - aI_{AA} - dI_{DD}) / I_{DD} \times I_{AA}$, where I_{DA} , I_{DD} , and I_{AA} are the background-subtracted FRET, CFP, and YFP images, respectively ($a = 0.0174$ and $d = 0.1729$). In a second method employed for time-lapse experiments in which dynamic changes in FRET in response to 2-APB stimulation were tracked, a simplified relative FRET approach was used to collect CFP and FRET images, and the ratio of signals obtained in the respective channels (I_{DA}/I_{DD}) upon 405-nm excitation was taken as evidence of a FRET change.

Intracellular Ca^{2+} measurements. Coverslips seeded with HeLa cells transiently co-transfected various vectors with the red genetically-encoded Ca^{2+} indicator CMV-R-GECO1.2 were placed in a perfusion chamber on the stage of an Olympus IX81 inverted microscope. Images were acquired at room temperature with a 40× or 60× oil objective (N.A. 1.4; Olympus), and images were analyzed with Fluoview software (Olympus). R-GECO1.2 were excited at 559 nm and the emission was recorded at 570–670 nm. Ca^{2+} fluctuations are reported as the fluorescence intensity of R-GECO1.2.

Results

Mutation of S417 abolishes STIM1 C-terminus interactions with Orai1.

The YFP-labelled whole STIM1 C-terminus (233–685) (ST1-CT-YFP) expression together with Orai1-CFP in HeLa cells led to a clear redistribution of ST1-CT-YFP with partial plasma membrane as well as cytosolic targeting (Fig. 1A). We measured fluorescence resonance energy transfer (FRET) between Orai1-CFP and ST1-CT-YFP, which demonstrated the direct interaction between whole STIM1 C-terminus and Orai1 (Fig. 1B). Confocal microscopy showed that The double-labelled whole STIM1 C-terminus (YFP-CT-CFP) coexpressed with Orai1-mKate was predominantly found at the PM whereas STIM1 C-terminus mutant (YFP-CT(S417G)-CFP)

expression together with Orai1-mKate was completely localized in the cytoplasm, indicating mutation of S417 abolishes STIM1 C-terminus interactions with Orai1 (Fig. 1C and D).

2-APB induces STIM1 C-terminus mutant(S417G) and Orai1 to undergo rapid reorganization into colocalized PM clusters.

Here, in HeLa cells coexpressing STIM1 C-terminus mutant (YFP-CT(S417G)-CFP) and Orai1-mKate, we found that the Orai1-mKate protein was exclusively and relatively uniformly located in the PM, and YFP-CT(S417G)-CFP was completely cytoplasmic before the addition of 2-APB (Fig. 1D, upper). 30 s after application of 50 μ M 2-APB, YFP-CT(S417G)-CFP redistributed to the PM, where it colocalized with Orai1-mKate, suggesting that the two proteins formed a complex (Fig. 1D, bottom); indeed, FRET experiments revealed a direct interaction between them (Fig. 7A).

To investigate the mechanism by which 2-APB restore the interaction between STIM1 C-terminus mutant(S417G) and Orai1, we constructed several STIM1-derived conformational sensors to monitor intramolecular rearrangements within the mutant STIM1 cytosolic portion during its interaction with Orai1. Each construct contained the CAD of STIM1, which is the key segment involved in this interaction (Fig. 2A). Expression of the constructs in HeLa cells revealed N-FRET values ranging between ~0.4 and ~0.1 (Fig. 2B).

S417 is required for STIM1-Orai1 binding and CRAC channel activation.

Exogenous expression of the CAD/SOAR domain along with Orai1 has been shown to result in constitutive colocalization and binding of CAD/SOAR to Orai1(Park et al., 2009; Yuan, Zeng, Dorwart, Choi, Worley & Muallem, 2009). Accordingly, we observed the robust resting N-FRET between Orai1-CFP and YFP-CAD(Fig.3C). By contrast, N-FRET between Orai1-CFP and mutant YFP-CAD(S417G) was strongly reduced(Fig.3C). Likewise, confocal microscopy showed that YFP-CAD-WT was predominantly found at the PM whereas YFP-CAD(S417G) was completely localized in the cytoplasm, indicating reduced binding of CAD(S417G) to Orai1 (Fig. 3A and B). To investigate whether the S417G mutation abolishes CRAC channel activation by CAD, we coexpressed Orai1 and WT or mutant CAD in HeLa cells. Whereas CAD-WT resulted in strong constitutive Ca^{2+} influx, mutant CAD-S417G failed to induce Ca^{2+} influx (Fig. 3 D-F).

A visible consequence of STIM1 oligomerization is the formation of STIM1 puncta at ER–PM junctions (Prakriya & Lewis, 2015; Soboloff, Rothberg, Madesh & Gill, 2012). We analyzed the role of S417 in CC3 for STIM1 puncta formation by time-lapse confocal microscopy in cells expressing WT or mutant (S417G) mCherry-STIM1 together with Orai1-YFP. In nonstimulated cells, STIM1-WT localized to the bulk ER away from the PM whereas Orai1 was distributed homogeneously in the PM (Fig. 4A). After ER store depletion with TG, STIM1-WT formed puncta, translocated to ER-PM junctions colocalized with Orai1 (Fig. 4A). Likewise, mutant STIM1-S417G was distributed diffusely in ER in resting cells (Fig. 4B). Surprisingly, upon store depletion, STIM1-S417G did not change its distribution and failed to redistribute into discrete puncta (Fig. 4B). In addition, the distribution of Orai1-YFP remained homogeneous after store depletion without signs of puncta formation and no significant colocalization with mCherry-STIM1-S417G (Fig. 4B). Consequently, mCherry-STIM1-WT resulted in strong Ca^{2+} influx, mCherry-STIM1-S417G failed to induce Ca^{2+} influx (Fig. 4C, D and E). Similar results were obtained in cells overexpressing S417E and S417L mutants (Data not shown). These results show that mutation of S417 abolishes STIM1 function.

2-APB dose-dependently activated Orai1 channel in stores-replete HeLa cells co-expressed STIM1 C-terminus mutant (S417G) and Orai1.

In our experiments, the red genetically-encoded Ca^{2+} indicator (GECI) CMV-R-GECO1.2 was chosen to examine the effect of different concentrations of 2-APB on cytosolic calcium in HeLa cells co-transfected with YFP-CT(S417G)-CFP, Orai1-CFP and CMV-R-GECO1.2 (Fig. 5A). As shown in Fig. 5B, despite stores remaining full, coexpression of double-labeled STIM1 C-terminus mutant (YFP-CT(S417G)-CFP) caused massive increases in Ca^{2+} entry, with the attainment of maximal Ca^{2+} peak upon the addition of higher concentrations of 2-APB (>20 μ M), followed by rapid inhibition. Instead, lower 2-APB concentrations (<5 μ M) appeared to potentiate but not inhibit Ca^{2+} influx. While cells overexpressing similar levels of Orai1-CFP or coexpressing Orai1-CFP and full length STIM1 showed little 2-APB-induced Ca^{2+} entry (data not shown). Additionally, using the green genetically encoded ER Ca^{2+}

indicator ER-GCaMP6, we demonstrated that concentrations of 2-APB in the range of 1~100 μ M did not affect the release of Ca²⁺ from intracellular stores in HeLa cells co-expressed YFP-CT(S417G)-CFP and Orai1-CFP. Consistent with previous studies, our patch clamp results also demonstrated that the massive 2-APB-induced Ca²⁺ entry represents authentic CRAC channel activity (data not shown).

2-APB induces the extension of STIM1 C-terminus mutant(S417G)

The YFP-CT(S417G)-CFP conformational sensor enabled us to investigate the molecular mechanism by which 2-APB induces the activation of Orai1 through its interaction with STIM1 C-terminus mutant(S417G). In HeLa cells transfected with YFP-CT(S417G)-CFP, YFP-CT(S417G)-CFP was uniformly expressed in the cytoplasm (Fig. S1D); a slight decrease in FRET was observed in the presence of 50 μ M 2-APB, suggesting rearrangement to an extended conformation (Fig. S1A-C). The YFP-CT(S417G)-CFP sensor formed cytosolic aggregates, but did not localize to the PM following 2-APB application (Fig. S1D). Treatment with 5 μ M 2-APB resulted in a slight FRET decrease, suggesting that the STIM1 C-terminus mutant(S417G) assumed an extended conformation even at a low concentration 2-APB (Fig. S1E, F). YFP-CT(S417G)-CFP still uniformly distributed in the cytoplasm when coexpressed with Orai1-mKate (Fig. S2D); however the YFP-CT(S417G)-CFP was rapidly localized to the PM upon the addition of 50 μ M 2-APB, which was accompanied by a slight decrease in FRET (Fig. S2A-C); a similar but less pronounced effect was observed by treatment with 5 μ M 2-APB (Fig. S2D-F). These data suggested the slightly extended conformation of STIM1 C-terminus mutant(S417G) induced by 2-APB may be potential mechanism for STIM1 CT(S417G)-Orai1 binding and CRAC channel activation.

The C- and N-terminal STIM1 binding sites on Orai1 are required for 2-APB-induced STIM1 C terminus mutant (S417G)-Orai1 coupling

2-APB appeared to promote the interaction of the STIM1 C-terminus mutant (S417G) and Orai1. To identify the sites in Orai1 that were involved in this interaction, we generated truncation constructs of Orai1-mKate lacking the cytoplasmic C-terminus (Orai1- Δ C-mKate) and N-terminus (Orai1- Δ N-mKate). YFP-CT(S417G)-CFP overexpressed in HeLa cells

redistributed from the cytoplasm to the PM where it co-localized with Orai1-mKate upon 2-APB application (Fig. S2A, D); moreover, both proteins exhibited an increase in FRET, suggesting a direct interaction between them (Fig. 7A, B). However, cytoplasmic YFP-CT(S417G)-CFP failed to colocalize with overexpressed Orai1- Δ C-mKate (a.a. 1–272) in the presence of 2-APB (Fig. 6A). Truncation of the cytoplasmic N-terminus of Orai1 (Orai1- Δ N-mKate; a.a. 90–301) also diminished the redistribution of YFP-CT(S417G)-CFP or its co-localization with Orai1- Δ N-mKate at the cell surface with 2-APB treatment (Fig. 6B), implying that mutations at the N-terminal site significantly impair 2-APB-induced STIM1 C-terminus mutant(S417G)-Orai1 coupling, although less significantly than mutations at the C-terminal site. To identify the motif within Orai1 that mediates this interaction, we generated Orai1 mutants with deletions in the CBD (Orai1- Δ CBD-mKate; Δ a.a. 272–292) or NBD (Orai1- Δ NBD-mKate; Δ a.a. 73–85). The results show that Δ CBD Orai1 mutations abolished STIM1 C-terminus mutant(S417G)-Orai1 association induced by 2-APB and Orai1- Δ NBD also significantly reduced these couplings (Fig. 6C, D and 7C–F). These findings indicate that both CBD and NBD of Orai1 mediate 2-APB-induced STIM1 C-terminus mutant(S417G)-Orai1 association.

Orai1 C-terminal residues L273 and L276 mediate coupling to STIM1 C terminus mutant(S417G) induced by 2-APB

Previous studies identified L273 and L276 in the C terminus of Orai1 as critical residues for interaction with STIM1. To assess the contribution of these residues to the STIM1 C terminus mutant(S417G)-Orai1 coupling induced by 2-APB, we generated two Orai1 mutants (Orai1-L273D-mKate and Orai1-L276D-mKate). Cytoplasmic YFP-CT(S417G)-CFP failed to colocalize with coexpressed Orai1-L273D-mKate or Orai1-L276D-mKate at the PM upon addition of 2-APB (Fig. 8). Consistent with this observation, FRET imaging revealed that there was no interaction between L273D or L276D mutant and STIM1 C terminus mutant(S417G) (data not shown). These results indicate that Orai1 L273 and L276 play key roles in the interaction of STIM1 C terminus mutant(S417G) and Orai1 induced by 2-APB.

Orai1 CBD and NBD are required for 2-APB-induced STIM1-CT mutant(S417G)-Orai1

binding and CRAC channel activation

For functional analyses, the original set of Orai1 mutants was cotransfected with YFP-CT(S417G)-CFP in HeLa cells. Constitutive Ca^{2+} entry in cells coexpressing YFP-CT(S417G)-CFP and Orai1-mKate was negligible; however, a massive increase was observed upon addition of 50 μM 2-APB, despite Ca^{2+} stores remaining full (Fig. 9A). In contrast to observations by confocal imaging, mutations (L273D or L276D) or truncations at either terminus of Orai1 (ΔNBD or ΔCBD) abolished 2-APB-triggered channel activity (Fig. 9B–F). These results indicate that both cytosolic portions of Orai1 are essential for 2-APB-mediated Orai1 activity.

2-APB induced STIM1-CT mutant(S417G)-Orai1-K85E binding and Orai1-K85E channel activation

Previous studies identified K85 in the N terminus of Orai1 as critical residues for store-operated gating of CRAC channels. To assess the contribution of this residue to the STIM1 C terminus mutant(S417G)–Orai1 coupling induced by 2-APB, we generated Orai1 mutants(Orai1-K85E-CFP and Orai1-K85E-mKate). The single point mutation of the cytoplasmic N-terminus of Orai1 (Orai1-K85E) obviously diminished the redistribution of YFP-CT(S417G)-CFP or its co-localization with Orai1-K85E at the cell surface with 2-APB treatment (Fig. 10A), implying that that this mutation at the N-terminal site significantly impair 2-APB-induced STIM1 C-terminus mutant(S417G)–Orai1 coupling, although less significantly than mutations at the C-terminal site of Orai1. Consistent with this observation, FRET imaging revealed that there was obviously diminished interaction between Orai1-K85E and STIM1 C terminus mutant(S417G) (Fig. 10B). We also choose the red genetically-encoded Ca^{2+} indicator (GECI) CMV-R-GECO1.2 to examine the effect of 2-APB on cytosolic calcium in HeLa cells co-transfected with YFP-CT(S417G)-CFP, Orai1-K85E-CFP and CMV-R-GECO1.2. As shown in Fig.10C, despite stores remaining full, coexpression of YFP-CT(S417G)-CFP with Orai1-CFP caused substantial increases in Ca^{2+} entry, with the attainment of maximal Ca^{2+} peak upon the addition of 50 μM 2-APB, followed by rapid inhibition. Instead, coexpression of YFP-CT(S417G)-CFP with Orai1-K85E-CFP appeared to significantly potentiate but not inhibit Ca^{2+} influx(Fig. 10D). We also found the

activation time of SOCE induced by 2-APB in cells coexpressing YFP-CT(S417G)-CFP and Orai1-K85E-CFP is greatly delayed compared with the cells coexpressing YFP-CT(S417G)-CFP and Orai1-WT.

Discussion

STIM1 is a type I single-span membrane protein which is located predominantly in the ER membrane (Grabmayr, Romanin & Fahrner, 2020; Liou et al., 2005; Roos et al., 2005; Zhang et al., 2005b). Function as a finely tuned ER Ca^{2+} sensor, STIM1 can undergo rapid and reversible translocation into close ER–PM junctions to couple with and activate Orai channels in the plasma membrane following store depletion (Grabmayr, Romanin & Fahrner, 2020; Prakriya & Lewis, 2015; Soboloff, Rothberg, Madesh & Gill, 2012). In order to perform these tasks, STIM1 is equipped with several specialized domains spread across its N- and C-terminal portions (Prakriya & Lewis, 2015; Soboloff, Rothberg, Madesh & Gill, 2012). Over the past years, a sophisticated model of Ca^{2+} -store-depletion-triggered STIM1 activation has been developed, emphasizing the role of both N- and C-terminal segments of STIM1. Recent evidence has provided support for the existence of two “brakes” (the EF-SAM domain itself and CC1 structural inhibitory clamp) on STIM1 activation (Ma et al., 2015; Muik et al., 2011; Yang, Jin, Cai, Li & Shen, 2012; Zhou et al., 2013). Ca^{2+} -store-depletion activates STIM1 by inducing the intra-dimeric binding of two EF-SAM domains, which triggers conformational changes in the transmembrane (TM) domain, propagates a series of downstream events including release of CAD/SOAR from CC1 inhibition and the consequent orai1 coupling and activation, (Prakriya & Lewis, 2015; Shim, Tirado-Lee & Prakriya, 2015). Although the interaction between CC1 and CAD controlling STIM1 activation is not fully understood, it is thought that CC1 and CC3 form an inhibitory clamp (Fahrner et al., 2014; Ma et al., 2015; Maus et al., 2015; Muik et al., 2011; Rathner et al., 2021). CAD (or SOAR) is recognized as the minimal region required for CRAC channel activation and have been documented to be sufficient to activate SOCs (Kawasaki, Lange & Feske, 2009; Park et al., 2009; Yuan, Zeng, Dorwart, Choi, Worley & Muallem, 2009). It contains two putative coiled-coil regions (CC2 and CC3) whose interaction helps to maintain each hairpin monomer in an inactive state (Park et al., 2009; Yang, Jin, Cai, Li & Shen, 2012). CC2 has been show to

establish the binding interactions with Orai1, which is a structurally best defined region in CAD (or SOAR) (Stathopoulos et al., 2013). However, the role of CC3 remains to be elucidated.

S417 is located in the third coiled-coil (CC3) domain of STIM1-CT. In our experiments, multiple kinds of YFP-labelled STIM1 (S417G) mutants of different length (containing amino acids 1-685, 233-685 and 342-488, respectively) were constructed to observe the interaction between STIM1 and Orai1. We found: Instead of clearly membrane targeting of STIM1 segments exhibited in cells co-expressing Orai1-CFP and STIM1-CT-YFP(amino acids, 233-685) or STIM1-CAD-YFP (amino acids, 342-448), either STIM1-CT or STIM1-CAD mutant of S417G led to itself completely localized in the cytoplasm. When expressed as full-length protein (amino acids, 1-685), STIM1 (S417G) mutants distributed diffusely in ER in resting cells and remained in ER and failed to aggregate into discrete puncta upon store depletion. Equally, the co-expressed Orai1-YFP still homogenously distributed within PM after store depletion, without signs of puncta formation and no significant co-localization with STIM1 (S417G) mutants. According to our data, mutation of S417 abolished PM localization of C terminus or CAD of STIM1, eliminating the FRET between STIM1-CT or CAD and Orai1 and the down-stream CAD-mediated Ca^{2+} influx. Which indicates that S417 and CC3 are critical for the binding of CAD to Orai1 and the following activation of CRAC channel. Maybe mutation of S417G in CC3 of STIM1 regulate the structure of the coiled-coil clamp involving the CC1 and CC3 domains which is essential in controlling STIM1 activation. But the exact mechanism by which S417 regulating the binding of STIM1 to Orai1 remains unclear, which needs high resolution structural data of the STIM1-CC3 and Orai1 complex to clarify.

2-APB was originally introduced as a membrane-permeant inhibitor of the IP3 receptor (Maruyama, Kanaji, Nakade, Kanno & Mikoshiba, 1997). Although it has subsequently been found to affect a variety of ion channels and transport processes, the most reliable and best-studied effect of 2-APB is its ability to affect the activity of CRAC channel (Bootman, Collins, Mackenzie, Roderick, Berridge & Peppiatt, 2002; Parekh & Putney, 2005). The mechanism of 2-APB action on CRAC channel still remains unclear, but the complex effects elicited by this drug suggests that it may target multiple processes of CRAC activation (Ali,

Xu & Xu, 2017; Bootman, Collins, Mackenzie, Roderick, Berridge & Peppiatt, 2002).

In our study, we were amazed to find that 2-APB restored the binding of STIM1 C-terminus(S417G) mutant to Orai1 and dose-dependently activated Orai1 channel (Fig.5). However, 2-APB failed to promote the interaction between Orai1- Δ CBD and STIM1 C-terminus(S417G) mutant (Fig.7). We also found that 2-APB could not cause STIM1-CT (S417G) mutants to redistribute and co-localize with L273D or L276D mutant of Orai1 at the PM (Fig.8). Both L273 and L276 have been recognized as the key residues for the hydrophobic interaction between Orai1 and STIM1 side chains (Li et al., 2011; Navarro-Borelly, Somasundaram, Yamashita, Ren, Miller & Prakriya, 2008), our finding suggested that L273 and L276 was crucial for 2-APB to trigger the STIM1-CT(S417G)-Orai1 coupling. And we showed that Orai1- Δ NBD could also impair the coupling, although its action seemed less significantly than that of Orai1- Δ CBD(Fig.7), but either terminus deletion of Orai1 markedly reduced the 2-APB-triggered Ca^{2+} entry(Fig.9), implying that both C- and N-terminal STIM1 binding sites of Orai1 are essential for STIM1-Orai1 coupling and SOCE. More than that, the decrease of FRET observed in cells transfected with double-labeled STIM1-CT (S417G), indicating a slightly extended conformation of STIM1-CT (Fig.S1). Hence, we supposed that 2-APB might initiate an intramolecular transition in STIM1-CT, thereby facilitate the binding with Orai1. Further investigation is needed to disclose the exact molecular mechanisms for 2-APB-induced STIM1-CT (S417G)-Orai1 coupling and Orai1 channel activation.

Several studies have shown that mutation of K85E in extended transmembrane N-terminal (ETON, amino acids 73–90) of Orai1 disabled the activation of CRAC channel (Derler et al., 2013; Lis, Zierler, Peinelt, Fleig & Penner, 2010; McNally, Somasundaram, Jairaman, Yamashita & Prakriya, 2013; Wei et al., 2016), despite this only slightly reduced STIM1 binding. But it is still debated whether the binding of STIM1 to Orai1 ETON is required for gating(Yeung, Yamashita & Prakriya, 2020). According to our data, the single point mutation of K85E in Orai1 substantially diminished the redistribution of YFP-CT (S417G)-CFP or its co-localization with Orai1-K85E at the cell surface upon 2-APB treatment (Fig.10A). Likewise, FRET imaging revealed obviously diminished interaction between Orai1-K85E and STIM1-CT mutant (S417G) (Fig. 10B). Which implying that K85E mutation significantly

impair 2-APB-induced STIM1-CT(S417G)-Orai1 coupling. Furthermore, according to our data, 50uM 2-APB induced maximal Ca^{2+} peak followed by rapid inhibition in cells co-expressing YFP-CT (S417G)-CFP and Orai1-WT-CFP (Fig.10C). Interestingly, in cells co-expressed YFP-CT(S417G)-CFP and Orai1-K85E-CFP, although the activation time of SOCE induced by 2-APB is greatly delayed, this drug still significantly potentiate but not inhibit Ca^{2+} influx(Fig.10D). These results support the idea that ETON region of Orai1 N-terminal is necessary for STIM1 binding and channel gating and K85 of ETON might mediate 2-APB's inhibition on SOCE activated by STIM1-bound Orai1.

In summary, we show that S417 in CC3 domain of STIM1 play an essential role for STIM1 function and activation of SOCE. We also present an experiment model of combined STM1 or Orai1 mutants with 2-APB for better understanding of SOCE activation. Our study confirms that both N- and C-termini of Orai1 are involved in channel gating and coupling with STIM1, and K85 of ETON region is essential in mediating 2-APB's inhibition on SOCE. Thus, our results provide new understanding on Orai1-activation by STIM1, important to in-depth study of molecular structure of CRAC channel and future drug design.

Acknowledgements

We are grateful to Professor Richard S. Lewis at Stanford University for the kind gift of mCherry-Stim1 plasmid. We thank Professor YH. Liao at Huazhong University of Science and Tecnology for Orai1-myc constructs. This work was supported by the National Natural Sciences Foundation of China (Grant No. 31371217) and National Natural Sciences Foundation of China (Grant No. 30871311).

Author contributions: Tao Yu, Xi Li, Huajing Liu, Jing Jin, Qianqian Luo, Shengjie Li and Jun He conducted the experiments. Jun He conceived the idea for the project, designed the experiments, analyzed and interpreted the results, wrote the paper with Tao Yu.

Conflict of interest: The authors declare that they have no conflicts of interest with the contents of this article.

References

- Ali S, Xu T, & Xu X (2017). CRAC channel gating and its modulation by STIM1 and 2-aminoethoxydiphenyl borate. *The Journal of physiology* 595: 3085-3095.
- Baba Y, Hayashi K, Fujii Y, Mizushima A, Watarai H, Wakamori M, *et al.* (2006). Coupling of STIM1 to store-operated Ca²⁺ entry through its constitutive and inducible movement in the endoplasmic reticulum. *Proceedings of the National Academy of Sciences of the United States of America* 103: 16704-16709.
- Böhm J, Chevessier F, De Paula AM, Koch C, Attarian S, Feger C, *et al.* (2013). Constitutive activation of the calcium sensor STIM1 causes tubular-aggregate myopathy. *The American Journal of Human Genetics* 92: 271-278.
- Bootman MD, Collins TJ, Mackenzie L, Roderick HL, Berridge MJ, & Peppiatt CM (2002). 2-aminoethoxydiphenyl borate (2-APB) is a reliable blocker of store-operated Ca²⁺ entry but an inconsistent inhibitor of InsP₃-induced Ca²⁺ release. *FASEB journal : official publication of the Federation of American Societies for Experimental Biology* 16: 1145-1150.
- Braun A, Varga-Szabo D, Kleinschnitz C, Pleines I, Bender M, Austinat M, *et al.* (2009). Orai1 (CRACM1) is the platelet SOC channel and essential for pathological thrombus formation. *Blood, The Journal of the American Society of Hematology* 113: 2056-2063.
- Derler I, Plenk P, Fahrner M, Muik M, Jardin I, Schindl R, *et al.* (2013). The Extended Transmembrane Orai1 N-Terminal (ETON) Region Combines Binding Interface and Gate for Orai1 Activation by STIM1*♦. *Journal of Biological Chemistry* 288: 29025-29034.
- Fahrner M, Muik M, Schindl R, Butorac C, Stathopoulos P, Zheng L, *et al.* (2014). A coiled-coil clamp controls both conformation and clustering of stromal interaction molecule 1 (STIM1). *Journal of Biological Chemistry* 289: 33231-33244.
- Feske S (2010). CRAC channelopathies. *Pflugers Archiv : European journal of physiology* 460: 417-435.
- Feske S, Gwack Y, Prakriya M, Srikanth S, Puppel S, Tanasa B, *et al.* (2006). A mutation in Orai1 causes immune deficiency by abrogating CRAC channel function. *Nature* 441: 179.
- Grabmayr H, Romanin C, & Fahrner M (2020). STIM proteins: an ever-expanding family. *International Journal of Molecular Sciences* 22: 378.
- Hogan PG, Lewis RS, & Rao A (2009). Molecular basis of calcium signaling in lymphocytes: STIM and ORAI. *Annual review of immunology* 28: 491-533.
- Kawasaki T, Lange I, & Feske S (2009). A minimal regulatory domain in the C terminus of STIM1 binds to and activates ORAI1 CRAC channels. *Biochemical and biophysical research communications* 385: 49-54.

Korzeniowski MK, Manjarrés IM, Varnai P, & Balla T (2010). Activation of STIM1-Orai1 involves an intramolecular switching mechanism. *Science signaling* 3: ra82-ra82.

Lacruz RS, & Feske S (2015). Diseases caused by mutations in ORAI1 and STIM1. *Annals of the New York Academy of Sciences* 1356.

Lee PJ, & Papachristou GI (2019). New insights into acute pancreatitis. *Nature reviews Gastroenterology & hepatology* 16: 479-496.

Li Z, Liu L, Deng Y, Ji W, Du W, Xu P, *et al.* (2011). Graded activation of CRAC channel by binding of different numbers of STIM1 to Orai1 subunits. *Cell research* 21: 305-315.

Liou J, Fivaz M, Inoue T, & Meyer T (2007). Live-cell imaging reveals sequential oligomerization and local plasma membrane targeting of stromal interaction molecule 1 after Ca²⁺ store depletion. *Proceedings of the National Academy of Sciences* 104: 9301-9306.

Liou J, Kim ML, Heo WD, Jones JT, Myers JW, Ferrell JE, Jr., *et al.* (2005). STIM is a Ca²⁺ sensor essential for Ca²⁺-store-depletion-triggered Ca²⁺ influx. *Current biology* : CB 15: 1235-1241.

Lis A, Zierler S, Peinelt C, Fleig A, & Penner R (2010). A single lysine in the N-terminal region of store-operated channels is critical for STIM1-mediated gating. *Journal of general physiology* 136: 673-686.

Lu T, Zhang Y, Su Y, Zhou D, & Xu Q (2022). Role of store-operated Ca²⁺ entry in cardiovascular disease. *Cell Communication and Signaling* 20: 1-10.

Ma G, Wei M, He L, Liu C, Wu B, Zhang SL, *et al.* (2015). Inside-out Ca²⁺ signalling prompted by STIM1 conformational switch. *Nature communications* 6: 7826.

Maruyama T, Kanaji T, Nakade S, Kanno T, & Mikoshiba K (1997). 2APB, 2-aminoethoxydiphenyl borate, a membrane-penetrable modulator of Ins(1,4,5)P₃-induced Ca²⁺ release. *Journal of biochemistry* 122: 498-505.

Maus M, Jairaman A, Stathopoulos PB, Muik M, Fahrner M, Weidinger C, *et al.* (2015). Missense mutation in immunodeficient patients shows the multifunctional roles of coiled-coil domain 3 (CC3) in STIM1 activation. *Proceedings of the National Academy of Sciences* 112: 6206-6211.

McNally BA, Somasundaram A, Jairaman A, Yamashita M, & Prakriya M (2013). The C- and N-terminal STIM1 binding sites on Orai1 are required for both trapping and gating CRAC channels. *The Journal of physiology* 591: 2833-2850.

Misceo D, Holmgren A, Louch WE, Holme PA, Mizobuchi M, Morales RJ, *et al.* (2014). A Dominant STIM1 Mutation Causes Sirminger Syndrome. *Human mutation* 35: 556-564.

Morin G, Biancalana V, Echaniz - Laguna A, Noury JB, Lornage X, Moggio M, *et al.* (2020). Tubular aggregate myopathy and Stormorken syndrome: Mutation spectrum and genotype/phenotype correlation. *Human Mutation* 41: 17-37.

Morin G, Bruechle NO, Singh AR, Knopp C, Jedraszak G, Elbracht M, *et al.* (2014). Gain - of - function mutation in STIM1 (P. R304W) is associated with Stormorken syndrome. *Human mutation* 35: 1221-1232.

Muik M, Fahrner M, Schindl R, Stathopoulos P, Frischauf I, Derler I, *et al.* (2011). STIM1 couples to ORAI1 via an intramolecular transition into an extended conformation. *The EMBO journal* 30: 1678-1689.

Navarro-Borelly L, Somasundaram A, Yamashita M, Ren D, Miller RJ, & Prakriya M (2008). STIM1-Orai1 interactions and Orai1 conformational changes revealed by live-cell FRET microscopy. *The Journal of physiology* 586: 5383-5401.

Nesin V, Wiley G, Kousi M, Ong E-C, Lehmann T, Nicholl DJ, *et al.* (2014). Activating mutations in STIM1 and ORAI1 cause overlapping syndromes of tubular myopathy and congenital miosis. *Proceedings of the National Academy of Sciences* 111: 4197-4202.

Parekh AB, & Putney JW, Jr. (2005). Store-operated calcium channels. *Physiological reviews* 85: 757-810.

Park CY, Hoover PJ, Mullins FM, Bachhawat P, Covington ED, Raunser S, *et al.* (2009). STIM1 clusters and activates CRAC channels via direct binding of a cytosolic domain to Orai1. *Cell* 136: 876-890.

Picard C, Mccarl CA, Papolos A, Khalil S, & Feske S (2009). STIM1 mutation associated with a syndrome of immunodeficiency and autoimmunity. *N Engl J Med* 360: 1971-1980.

Prakriya M, & Lewis RS (2015). Store-Operated Calcium Channels. *Physiological reviews* 95: 1383-1436.

Rathner P, Fahrner M, Cerofolini L, Grabmayr H, Horvath F, Krobath H, *et al.* (2021). Interhelical interactions within the STIM1 CC1 domain modulate CRAC channel activation. *Nature chemical biology* 17: 196-204.

Roos J, DiGregorio PJ, Yeromin AV, Ohlsen K, Lioudyno M, Zhang S, *et al.* (2005). STIM1, an essential and conserved component of store-operated Ca²⁺ channel function. *The Journal of cell biology* 169: 435-445.

Shaw PJ, Qu B, Hoth M, & Feske S (2013). Molecular regulation of CRAC channels and their role in lymphocyte function. *Cellular and molecular life sciences* 70: 2637-2656.

Shim AH, Tirado-Lee L, & Prakriya M (2015). Structural and functional mechanisms of CRAC channel regulation. *Journal of molecular biology* 427: 77-93.

Soboloff J, Rothberg BS, Madesh M, & Gill DL (2012). STIM proteins: dynamic calcium signal transducers. *Nature reviews Molecular cell biology* 13: 549-565.

Stathopoulos PB, Schindl R, Fahrner M, Zheng L, Gasmi-Seabrook GM, Muik M, *et al.* (2013). STIM1/Orai1 coiled-coil interplay in the regulation of store-operated calcium entry. *Nature communications* 4: 1-12.

Varga-Szabo D, Braun A, Kleinschnitz C, Bender M, Pleines I, Pham M, *et al.* (2008). The calcium sensor STIM1 is an essential mediator of arterial thrombosis and ischemic brain infarction. *The Journal of experimental medicine* 205: 1583-1591.

Wei M, Zhou Y, Sun A, Ma G, He L, Zhou L, *et al.* (2016). Molecular mechanisms underlying inhibition of STIM1-Orai1-mediated Ca²⁺ entry induced by 2-aminoethoxydiphenyl borate. *Pflügers Archiv-European Journal of Physiology* 468: 2061-2074.

Wu MM, Covington ED, & Lewis RS (2014). Single-molecule analysis of diffusion and trapping of STIM1 and Orai1 at endoplasmic reticulum-plasma membrane junctions. *Molecular biology of the cell* 25: 3672-3685.

Yang S, Zhang JJ, & Huang X-Y (2009). Orai1 and STIM1 are critical for breast tumor cell migration and metastasis. *Cancer cell* 15: 124-134.

Yang X, Jin H, Cai X, Li S, & Shen Y (2012). Structural and mechanistic insights into the activation of Stromal interaction molecule 1 (STIM1). *Proceedings of the National Academy of Sciences of the United States of America* 109: 5657-5662.

Yeung PSW, Yamashita M, & Prakriya M (2020). Molecular basis of allosteric Orai1 channel activation by STIM1. *The Journal of physiology* 598: 1707-1723.

Yu F, Sun L, Hubrack S, Selvaraj S, & Machaca K (2013). Intramolecular shielding maintains the ER Ca²⁺ sensor STIM1 in an inactive conformation. *Journal of cell science* 126: 2401-2410.

Yuan JP, Zeng W, Dorwart MR, Choi YJ, Worley PF, & Muallem S (2009). SOAR and the polybasic STIM1 domains gate and regulate Orai channels. *Nature cell biology* 11: 337-343.

Zhang SL, Yu Y, Roos J, Kozak JA, Deerinck TJ, Ellisman MH, *et al.* (2005a). STIM1 is a Ca²⁺ sensor that activates CRAC channels and migrates from the Ca²⁺ store to the plasma membrane. *Nature* 437: 902-905.

Zhang SL, Yu Y, Roos J, Kozak JA, Deerinck TJ, Ellisman MH, *et al.* (2005b). STIM1 is a Ca²⁺

sensor that activates CRAC channels and migrates from the Ca²⁺ store to the plasma membrane. Nature 437: 902-905.

Zhou Y, Srinivasan P, Razavi S, Seymour S, Meraner P, Gudlur A, *et al.* (2013). Initial activation of STIM1, the regulator of store-operated calcium entry. Nature structural & molecular biology 20: 973-981.

Zhu Z-D, Yu T, Liu H-J, Jin J, & He J (2018). SOCE induced calcium overload regulates autophagy in acute pancreatitis via calcineurin activation. Cell death & disease 9: 1-12.

Figure Legends

Figure 1. S417 mutation abolishes STIM1 C-terminus-Orai1 interaction. (A) YFP-labelled whole STIM1 C-terminus(ST1-CT-YFP) coexpressed with Orai1-CFP in HeLa cells exhibited clearly membrane targeting. Line-scan intensity plots show the distribution of ST1-CT-YFP (green lines) and Orai1-CFP (blue line). (B) N-FRET live cell images of HeLa cells coexpressing ST1-CT-YFP and Orai1-CFP. (C) The double-labelled whole STIM1 C-terminus(YFP-CT-CFP) expression together with Orai1-mKate also exhibited clearly membrane targeting. Line-scan intensity plots show the distribution of YFP-CT-CFP (green lines) and Orai1-mKate (red line). (D) YFP-CT(S417G)-CFP coexpressed with Orai1-mKate in HeLa cells was redistributed from the cytoplasm to the PM upon application of 50 μ M 2-APB. Line-scan intensity plots show the distribution of YFP-CT(S417G)-CFP (green lines) and Orai1-mKate (red line) before (upper panel) and 5 min after (lower panel) application of 50 μ M 2-APB.

Figure 2. (A) STIM1 mutation-derived conformational sensor design. Schematic illustration of STIM1 protein and conformational sensors used in these studies. YFP-CT(S417G)-CFP contains the complete STIM1 C terminus(S417G); YFP-OASF(S417G)-CFP is the OASF(S417G) region; and YFP-CAD(S417G)-CFP comprises the CAD(S417G) of STIM1. All proteins were labeled with YFP/CFP as shown. (B) Localization and calculated N-FRET live cell image series of STIM1 fragment mutants 342–448 (CAD), 233–474 (OASF), and 233–685 (complete STIM1 C terminus). (E) Block diagram summarizing intramolecular N-FRET of YFP-STIM1-CFP fragment mutants 342–448, 233–474, and 233–685. *P < 0.05; **P < 0.001.

Figure 3. S417 mutation abolishes CAD-Orai1 interaction. (A) Representative Confocal images

of HeLa cells coexpressing YFP-CAD and Orai1-mKate. Line-scan intensity plots show the distribution of YFP-CAD (green lines) and Orai1-mKate (red line). (B) Representative Confocal images of cells coexpressing YFP-CAD(S417G) and Orai1-mKate. Line-scan intensity plots show the distribution of YFP-CAD(S417G) (green lines) and Orai1-mKate (red line). (C) Averaged N-FRET of Orai1-CFP and WT or mutant (S417G) YFP-CAD expressed in HeLa cells without TG stimulation in 0mM Ca^{2+} . (D and E) Ca^{2+} influx in HeLa cells coexpressing Orai1 and WT-CAD (D) or mutant CAD-S417G (E). (F) Averaged peak $[Ca^{2+}]_i$ values associated with Ca^{2+} influx in HeLa cells coexpressing Orai1 and WT-CAD or mutant CAD-S417G shown in panels D and E. * $P < 0.05$; ** $P < 0.001$.

Figure 4. S417 is essential for STIM1 puncta formation and colocalization with Orai1. (A and B) Representative Confocal images of HeLa cells expressing Orai1-YFP and WT or mutant (S417G) mCherry-STIM1 before and after stimulation with 1 μ M TG in Ca^{2+} -free Ringer's solution for 5 min. Line-scan intensity plots show the distribution of WT or mutant (S417G) mCherry-STIM1 (red lines) and Orai1-mKate (green line) before (upper panel) and 5 min after (lower panel) application of 1 μ M TG. (C and D) TG-induced SOCE in HeLa cells coexpressing Orai1 and WT-STIM1 (C) or mutant STIM1-S417G (D). (F) Averaged peak $[Ca^{2+}]_i$ values associated with SOCE in HeLa cells coexpressing Orai1 and WT-STIM1 or mutant STIM1-S417G shown in panels C and D. * $P < 0.05$; ** $P < 0.001$.

Figure 5. 2-APB dose-dependently induced large Ca^{2+} entry in HeLa cells co-transfected with YFP-CT(S417G)-CFP and Orai1-CFP. HeLa cells were co-transfected with YFP-CT(S417G)-CFP, Orai1-CFP and CMV-R-GECO1.2 constructs. After 48 h, live cells were examined in a confocal microscope. (A) Representative Confocal images of HeLa cells coexpressing YFP-CT(S417G)-CFP, Orai1-CFP and CMV-R-GECO1.2 before and after application of 50 μ M 2-APB. (B) Different concentration 2-APB-induced Ca^{2+} influx reported by the red genetically-encoded Ca^{2+} indicator (GECI) CMV-R-GECO1.2. (C) Four pseudo-color images of CMV-R-GECO1.2 fluorescence in live cells acquired at 0 sec, 446 sec, 500sec, and 600 sec, respectively.

Figure 6. Both CBD and NBD of Orai1 is required for 2-APB-induced coupling between STIM1 C terminus mutant(S417G) and Orai1. (A-D left) Representative fluorescent images of the indicated YFP-CT(S417G)-CFP construct coexpressed with the indicated Orai1 mutants

before and after application of 2-APB (50 μ M). Note that when co-expressed with Orai1- Δ N-mKate or Orai1- Δ NBD-mKate, but not with Orai1- Δ C-mKate or Orai1- Δ CBD-mKate, the cellular distribution of YFP-CT-CFP is changed following the addition of 2-APB. However, the redistribution of YFP-CT(S417G)-CFP coexpressed these N-terminal mutants is weaker than coexpressed WT Orai1. (A-D right) Line-scan intensity plots depicting the distribution of YFP-CT(S417G)-CFP (green line) and Orai1 mutants (red line) between the cytosol and PM, as indicated by the solid line before (upper panel) and 5 min after (lower panel) application of 2-APB.

Figure 7. Interaction between Orai1 and STIM1 C terminus mutant(S417G) induced by 2-APB depends on the CBD and NBD of Orai1. (A) Localization and N-FRET live cell images of HeLa cells coexpressing YFP-CT(S417G)-CFP and Orai1-YFP. (B) Block diagram of calculated N-FRET in the PM. (C) Localization and N-FRET live cell images of cells coexpressing YFP-CT(S417G)-CFP and Orai1- Δ CBD-YFP. (D) Block diagram of calculated N-FRET for the PM. (E) Localization and N-FRET live cell images of cells coexpressing YFP-CT(S417G)-CFP and Orai1- Δ NBD-YFP. (F) Block diagram summarizing calculated N-FRET for the PM. *P < 0.05; **P < 0.001.

Figure 8. Orai1 L273D or L276D mutant show disrupted 2-APB-induced association with the STIM1 C terminus mutant(S417G). (A) YFP-CT(S417G)-CFP coexpressed with Orai1-L273D-mKate in HeLa cells failed to redistribute from the cytoplasm to the PM in the presence of 50 μ M 2-APB. Line-scan intensity plots depicting the distribution of YFP-CT(S417G)-CFP (green line) and Orai1-L273D-mKate (red line) between the cytosol and PM, as indicated by the solid line before (upper panel) and 5 min after (lower panel) application of 50 μ M 2-APB. (B) 2-APB failed to induce redistribution of YFP-CT(S417G)-CFP and its interaction with Orai1-L276D-mKate. Line-scan intensity plots depicting the redistribution of YFP-CT(S417G)-CFP (green line) and Orai1-L276D-mKate (red line) between the cytosol and PM, as indicated by the solid line before (upper panel) and 5 min after (lower panel) application of 50 μ M 2-APB.

Figure 9. Both the CBD and NBD of Orai1 are indispensable for 2-APB-mediated STIM1-CT mutant(S417G)-Orai1 binding and Orai1 activation. (A–C) Representative intracellular free Ca²⁺ traces show 2-APB-triggered Ca²⁺ entry in HeLa cells transfected with

(i) YFP-CT(S417G)-CFP+Orai1-mKate; (ii) YFP-CT(S417G)-CFP+Orai1- Δ NBD-mKate; and (iii) YFP-CT(S417G)-CFP +Orai1- Δ CBD-mKate. (D) Averaged peak $[Ca^{2+}]_i$ values associated with 2-APB-triggered Ca^{2+} influx in cells coexpressing YFP-CT(S417G)-CFP with wild-type or mutant Orai1 shown in panels A–E. *P < 0.05; **P < 0.001.

Figure 10. 2-APB induced STIM1-CT mutant(S417G)-Orai1-K85E binding and Orai1-K85E channel activation. (A) Representative Confocal images of HeLa cells coexpressing YFP-CT(S417G)-CFP with Orai1-K85E-CFP before (upper panel) and 5 min after (lower panel) application of 50 μ M 2-APB. Line-scan intensity plots show the distribution of Orai1-K85E-CFP (green lines) and YFP-CT(S417G)-CFP (red line). (B) Averaged N-FRET of Orai1-K85E-CFP and YFP-CT(S417G)-CFP expressed in HeLa cells before and 5 min after application of 50 μ M 2-APB. (C and D) 2-APB-induced Ca^{2+} influx in HeLa cells coexpressing YFP-CT(S417G)-CFP and WT-Orai1(C) or mutant Orai1-K85E (D). (E) Averaged peak $[Ca^{2+}]_i$ values associated with Ca^{2+} influx induced by 2-APB in cells coexpressing YFP-CT(S417G)-CFP and WT-Orai1(C) or mutant Orai1-K85E (from left to right, n = 28 and 28 cells) shown in panels C and D. (F) Averaged activation time associated with Ca^{2+} influx induced by 2-APB in cells coexpressing YFP-CT(S417G)-CFP and WT-Orai1(C) or mutant Orai1-K85E shown in panels C and D. *P < 0.05; **P < 0.001.

Supplementary figure legends

Figure S1. 2-APB dose-dependently induces a decrease in FRET in HeLa cells transfected with double-labeled STIM1 C terminus mutant(YFP-CT(S417G)-CFP). (A) CFP and FRET live cell image series and (B) relative FRET traces of YFP-CT(S417G)-CFP-expressing cells stimulated with 50 μ M 2-APB. In (B), values were normalized to resting FRET levels before 2-APB treatment. (C) Block diagram comparing resting and maximum FRET following treatment with 50 μ M 2-APB. (D) Redistribution of CFP and YFP fluorescence in YFP-CT(S417G)-CFP-transfected cells treated with 50 μ M 2-APB. The magnified image in the white box shows cytosolic aggregates formed by the STIM1 C terminus mutant (right panel). (E) Time course of relative FRET and (F) block diagram comparing resting and maximum FRET in YFP-CT(S417G)-CFP upon application of 5 μ M 2-APB. *P < 0.05; **P < 0.001.

Figure S2. Redistribution of double-labeled STIM1-CT mutant (S417G) and its interaction

with Orai1-mKate induced by 2-APB. (A) YFP-CT(S417G)-CFP coexpressed with Orai1-mKate in HeLa cells was redistributed from the cytoplasm to the PM upon application of 50 μ M 2-APB. Line-scan intensity plots show the distribution of YFP-CT(S417G)-CFP (blue and green lines) and Orai1-mKate (red line) before (upper panel) and 5 min after (lower panel) application of 50 μ M 2-APB. (B) Time course of relative FRET and (C) block diagram comparing resting and maximum FRET of YFP-CT(S417G)-CFP in the presence of 50 μ M 2-APB. Values were normalized to resting FRET levels before 2-APB treatment. (D) Redistribution of YFP-CT(S417G)-CFP coexpressed with Orai1-mKate from the cytoplasm to the PM by treatment with 5 μ M 2-APB. Line-scan intensity plots show the distribution of YFP-CT(S417G)-CFP (blue and green lines) and Orai1-mKate (red line) before (upper panel) and 5 min after (lower panel) application of 5 μ M 2-APB. (E) Time course of relative FRET of YFP-CT(S417G)-CFP in the presence of 5 μ M 2-APB. Values were normalized to resting FRET levels before 2-APB treatment. (F) Block diagram comparing resting and maximum FRET of YFP-CT(S417G)-CFP in the presence of 5 μ M 2-APB. *P < 0.05; **P < 0.001.

Figure 1

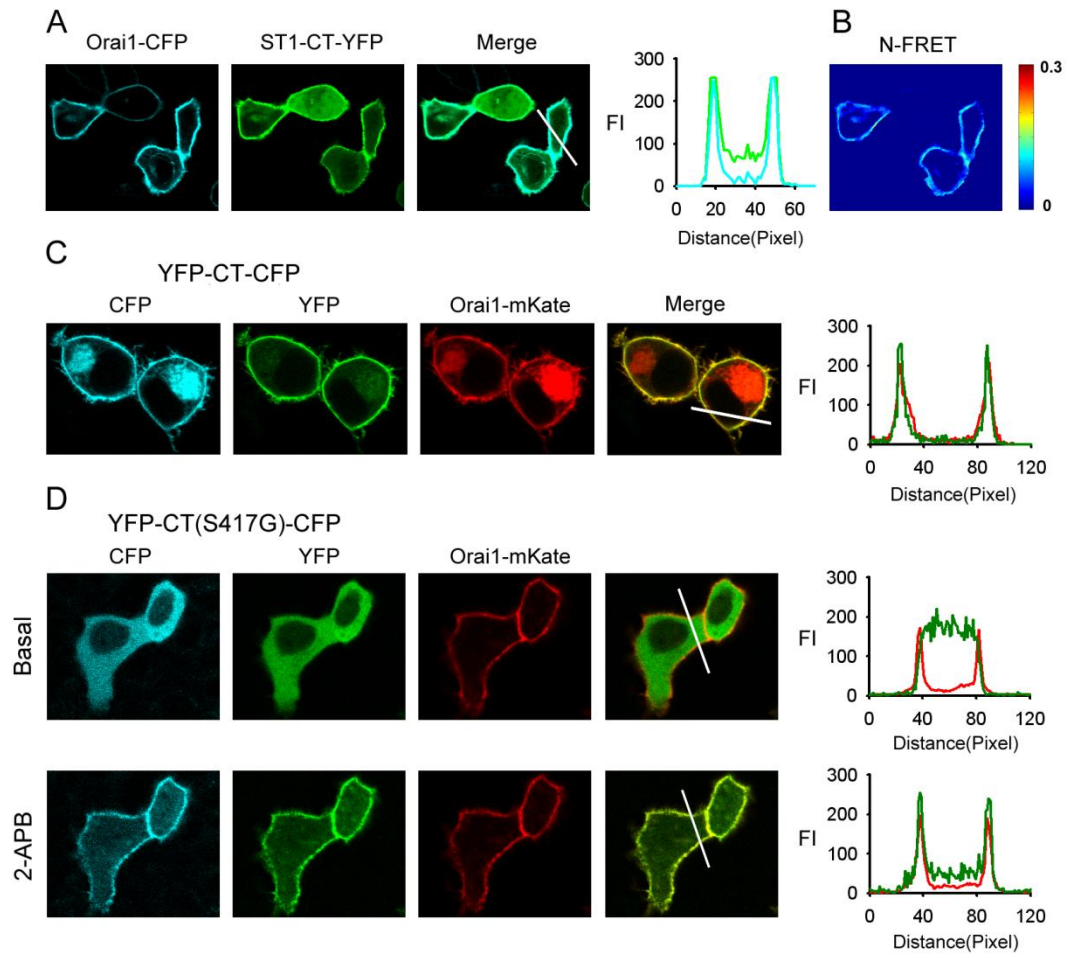


Figure 2

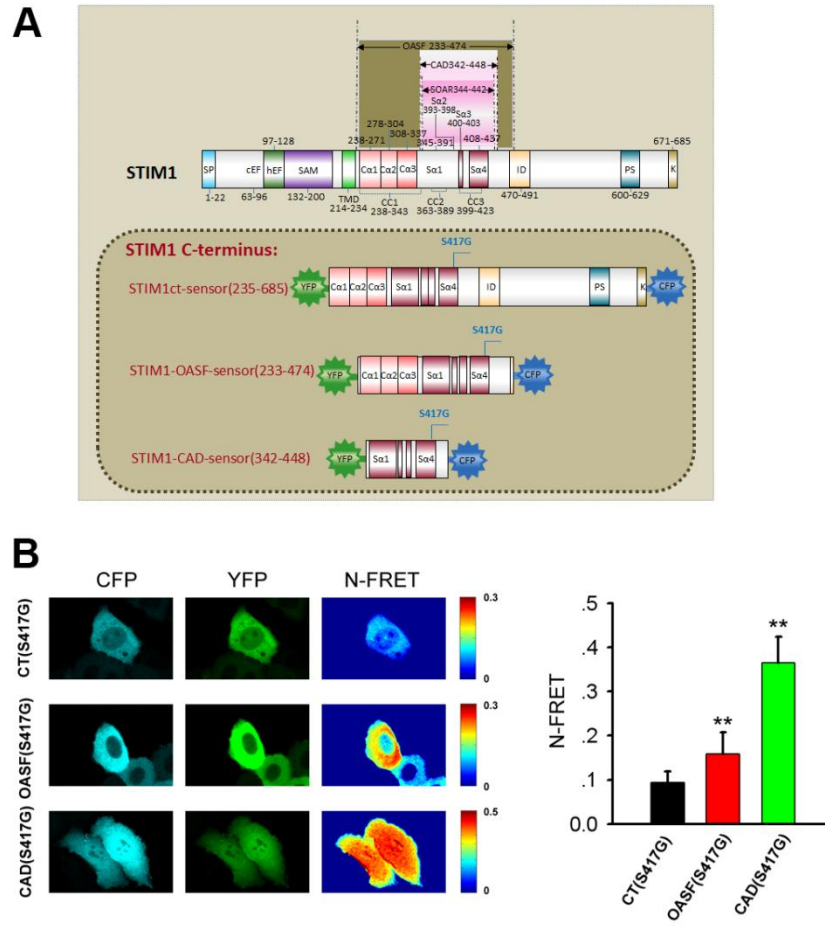


Figure 3

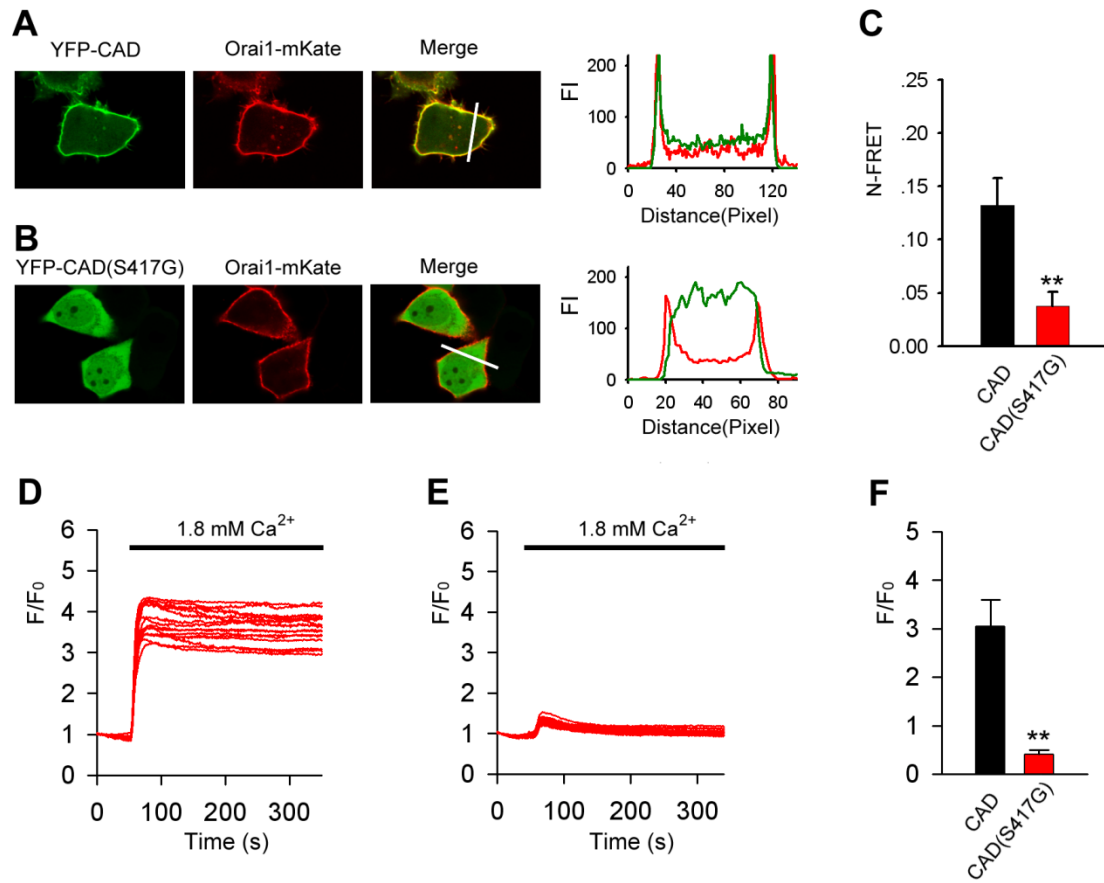


Figure 4

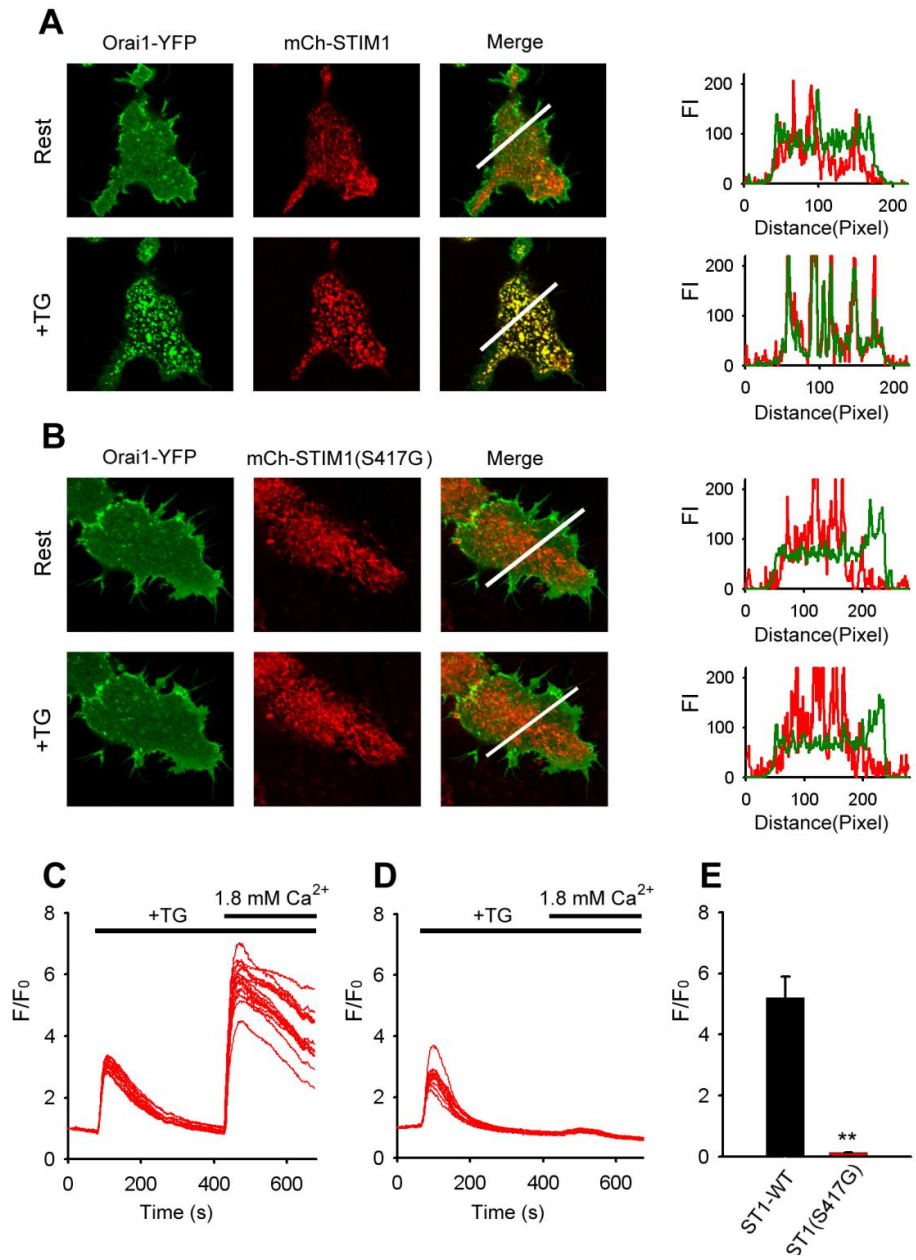


Figure 5

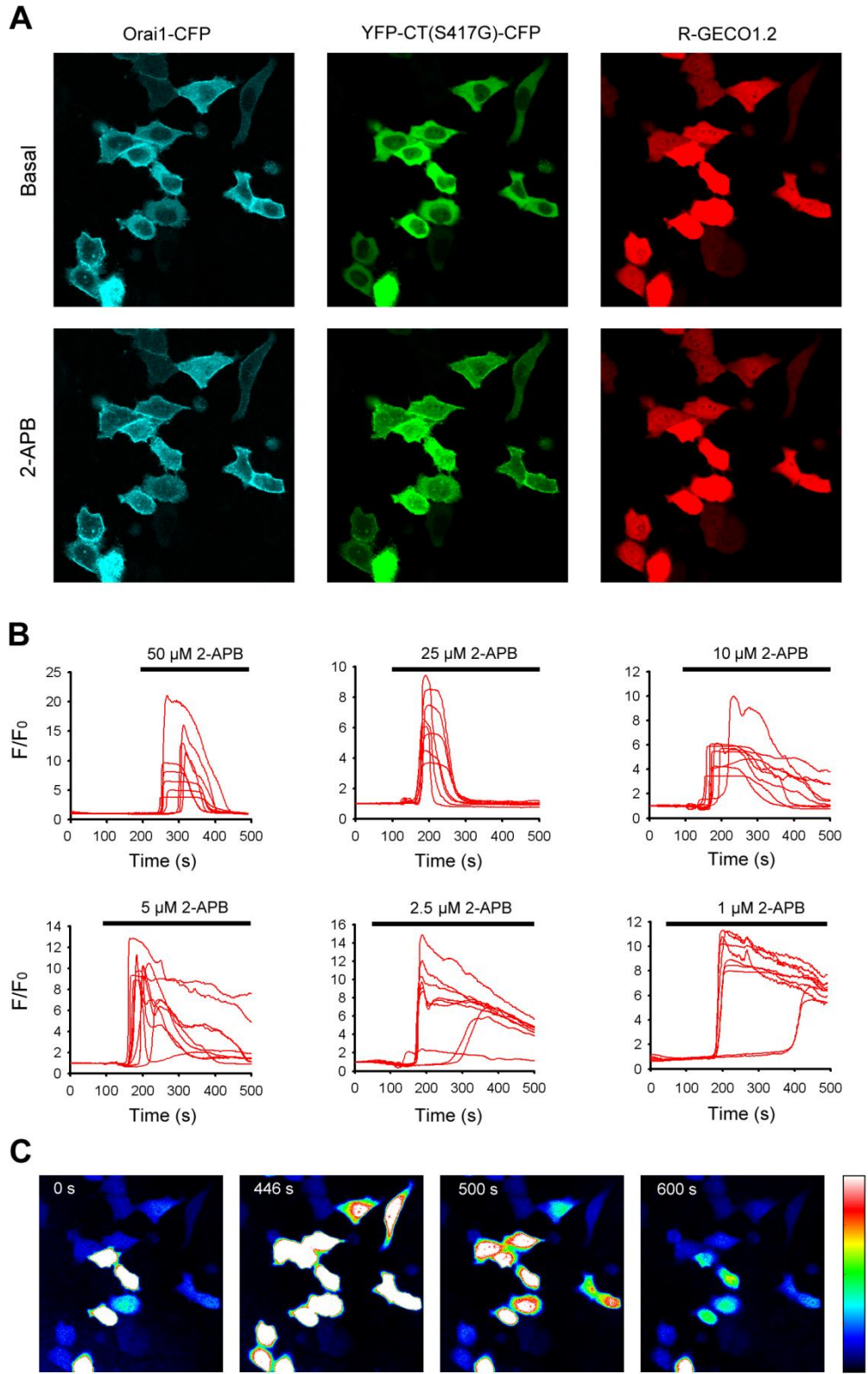


Figure 6

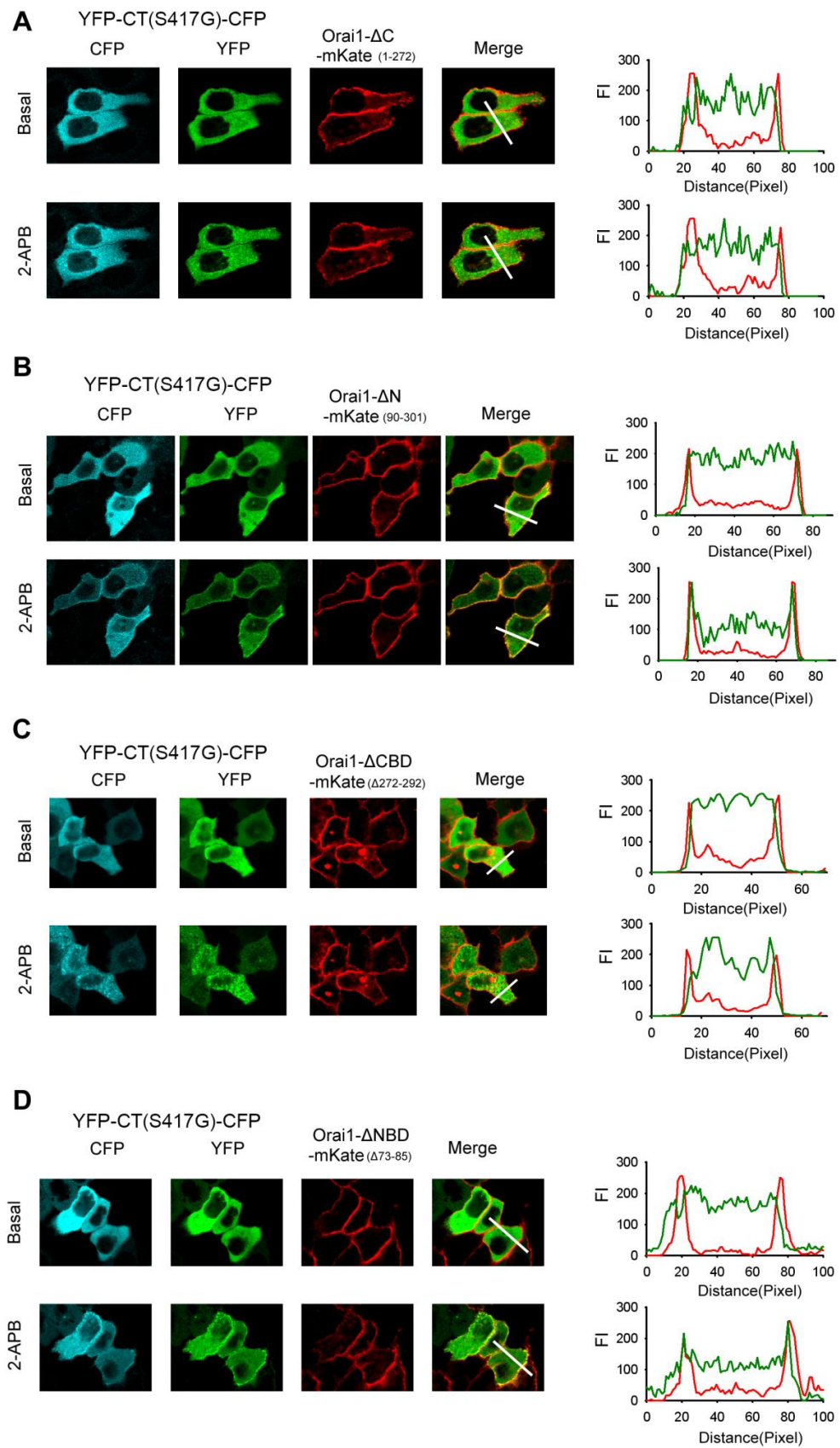


Figure 7

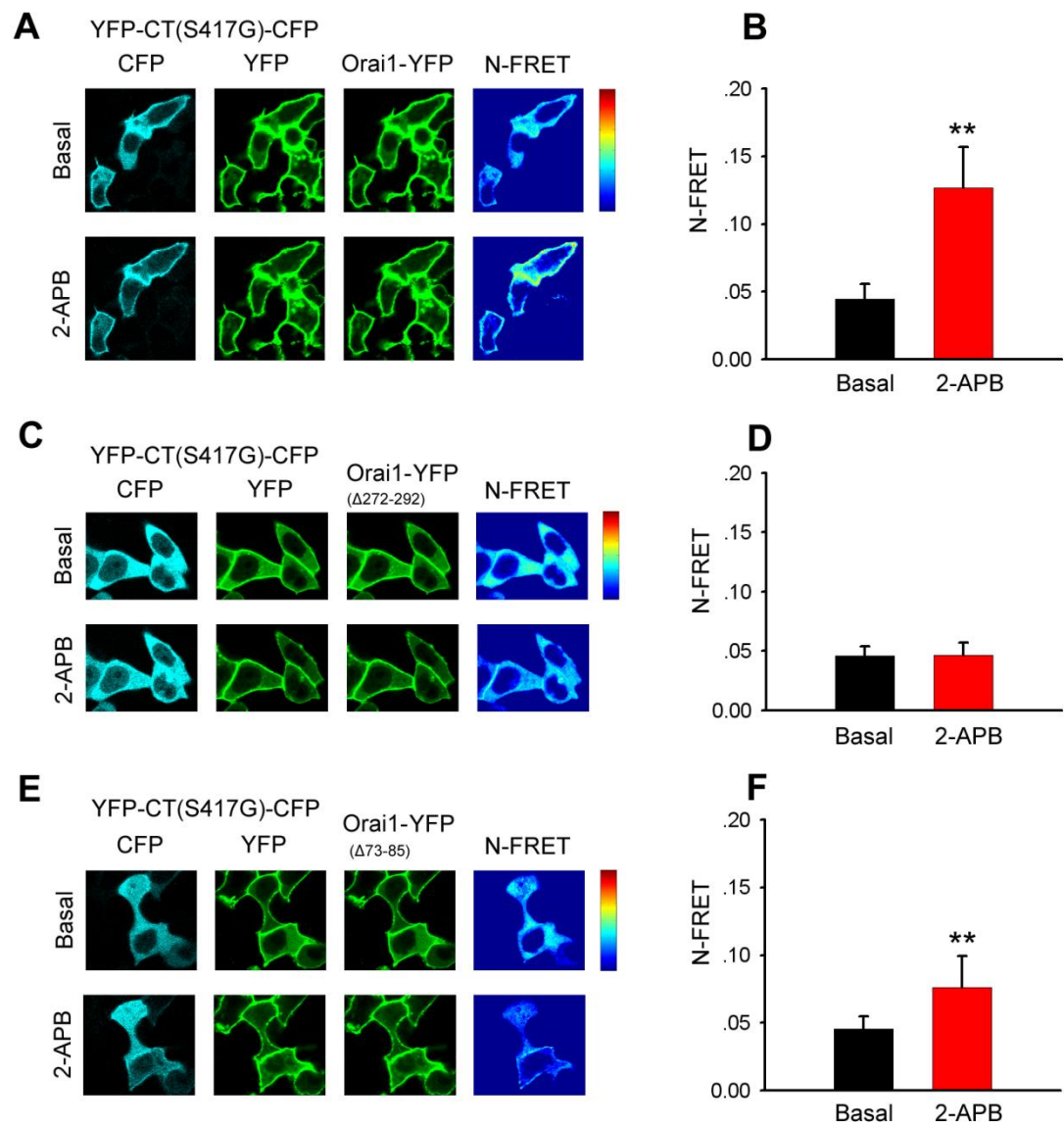


Figure 8

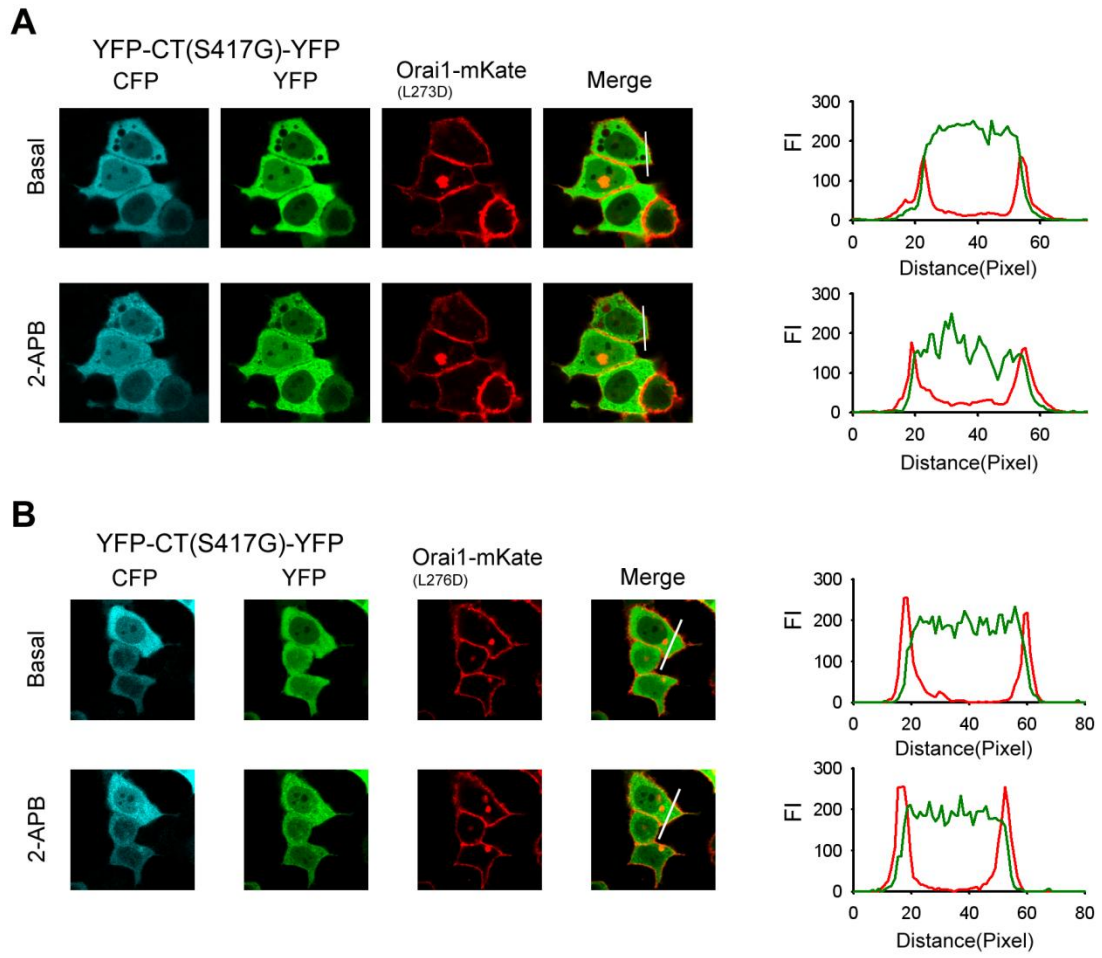


Figure 9

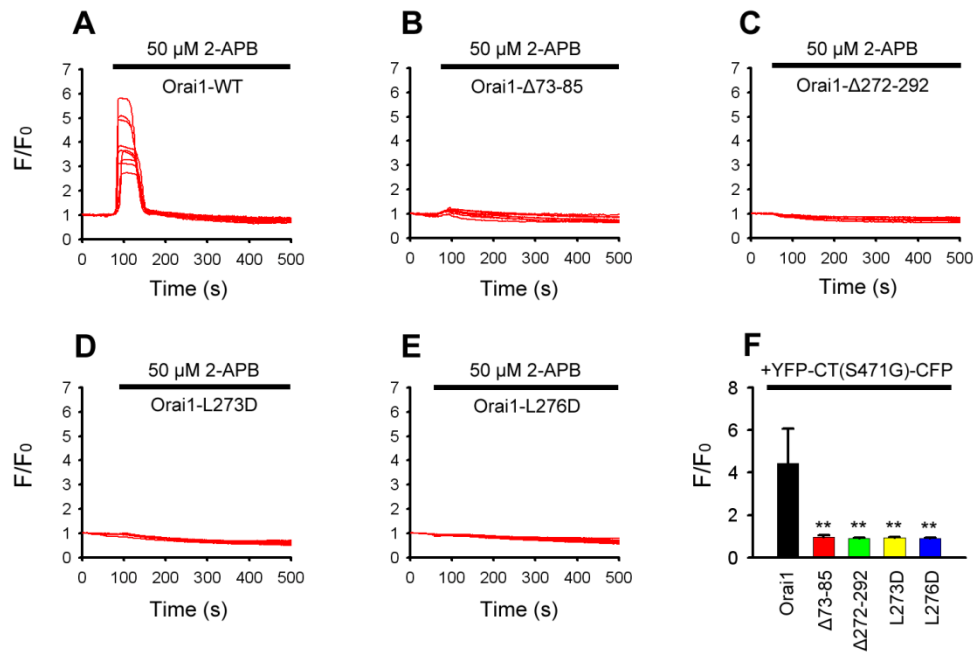


Figure 10

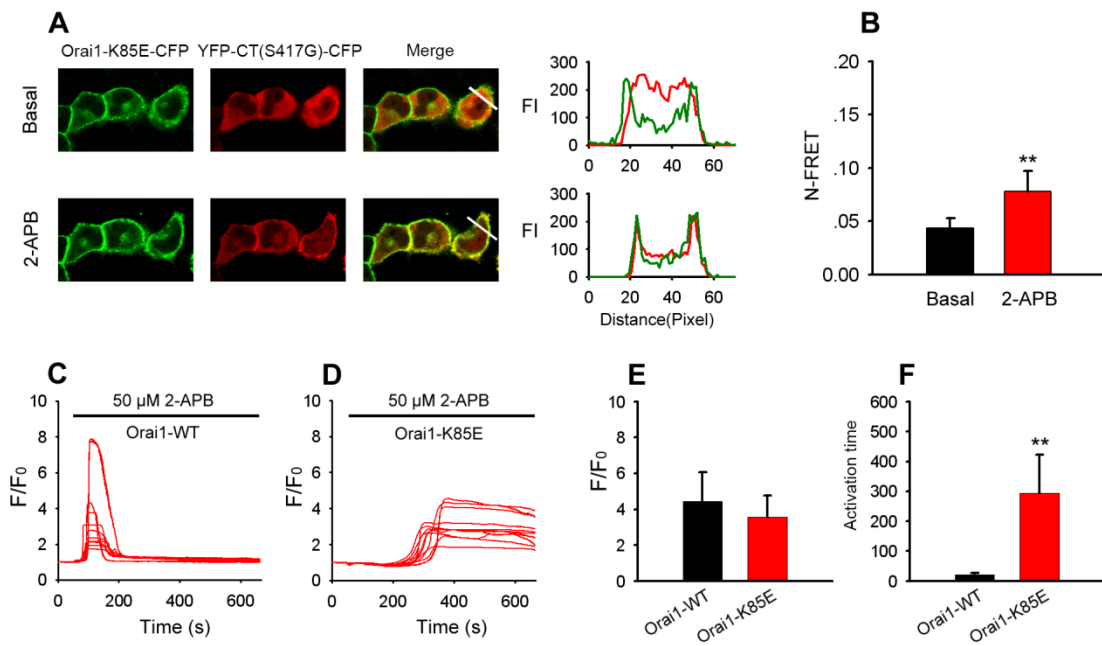


Figure S1

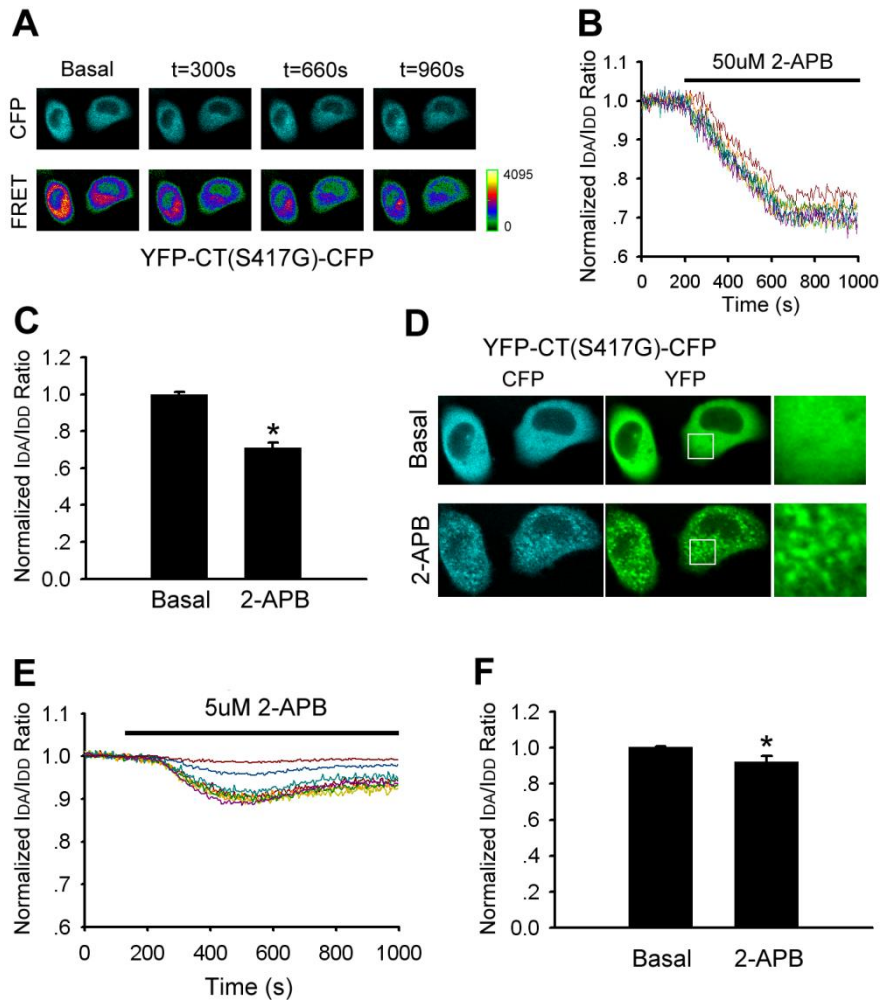


Figure S2

